# Learning Mixed Quantum States in Large-Scale Experiments

Matteo Votto,[1,*] Marko Ljubotina,[2,3,4] Cécilia Lancien,[5] J. Ignacio Cirac,[6,3] Peter Zoller,[7,8] Maksym Serbyn,[4] Lorenzo Piroli,[9] and Benoît Vermersch[1,10]

[1]*Université Grenoble Alpes, CNRS, LPMMC, 38000 Grenoble, France*

[2]*Technical University of Munich, TUM School of Natural Sciences, Physics Department, James-Franck-Straße 1, 85748 Garching, Germany*

[3]*Munich Center for Quantum Science and Technology (MCQST), Schellingstraße 4, 80799 München, Germany*

[4]*Institute of Science and Technology Austria (ISTA), Am Campus 1, 3400 Klosterneuburg, Austria*

[5]*Université Grenoble Alpes, CNRS, Institut Fourier, 38610 Gières, France*

[6]*Max Planck Institute of Quantum Optics, Hans-Kopfermann-straße 1, Garching 85748, Germany*

[7]*Institute for Theoretical Physics, University of Innsbruck, Innsbruck A-6020, Austria*

[8]*Institute for Quantum Optics and Quantum Information of the Austrian Academy of Sciences, Innsbruck A-6020, Austria*

[9]*Dipartimento di Fisica e Astronomia, Università di Bologna and INFN, Sezione di Bologna, via Irnerio 46, I-40126 Bologna, Italy*

[10]*Quobly, Grenoble, France*

(Received 25 July 2025; revised 13 November 2025; accepted 2 January 2026; published 4 March 2026)

We present and test a protocol to learn the matrix-product operator (MPO) representation of an experimentally prepared quantum state. The protocol takes as input classical shadows corresponding to local randomized measurements, and outputs the tensors of an MPO maximizing a suitably defined fidelity with the experimental state. The tensor optimization is carried out sequentially, similarly to the well-known density matrix renormalization group algorithm. Our approach is provably efficient under certain technical conditions expected to be met in short-range correlated states and in typical noisy experimental settings. Under the same conditions, we also provide an efficient scheme to estimate fidelities between the learned and the experimental states. We experimentally demonstrate our protocol by learning entangled quantum states of up to $N = 96$ qubits in a superconducting quantum processor. Our method upgrades classical shadows to large-scale quantum computation and simulation experiments.

DOI: 10.1103/rbg2-f61m

Probing the quantum state of an $N-$ qubit system is a crucial yet non-trivial step in the successful implementation of many quantum simulation and quantum computation protocols [1–11]. In this context, randomized measurements provide an effective strategy to probe several physical properties of experimental quantum systems [12–14], such as entanglement [15–21] and fidelities [22–26]. In particular, the framework of classical shadows [27] has become a routine tool to postprocess randomized measurement datasets. This is due to (i) provable performance guarantees for statistical errors, that allow us to reach considerable system sizes [21–23,27], (ii) minimal hardware requirements (applying one layer of single-qubit unitaries before measurements suffices) [13], and (iii) robustness to measurement errors [28–30]. While classical shadows are state-agnostic, typical quantum states generated in noisy quantum devices admit simple descriptions. For instance, matrix-product operators (MPOs) can accurately describe output states of one-dimensional noisy quantum circuits [31,32], as well as one-dimensional thermal states relevant to quantum simulation [33,34], with only $O(N)$ parameters. However, it remains unclear how to efficiently reconstruct such quantum states from classical shadows at large system sizes.

In this Letter, we introduce a protocol to learn the MPO representation of quantum states in large-scale experiments, which inherits the key properties (i)–(iii) of classical shadows. This allows us to probe global properties of quantum states with extensive entropies in experimental settings. We show this by learning many-body states generated by a superconducting quantum processor up to $N = 96$ qubits, whereas randomized measurements have been previously implemented only up to $N = 13$ [30]. The MPO representation provides direct access to several physical properties [35], without the need for tailored estimation formulas, nor to reprocess the dataset as in previous approaches [13]. Leveraging this full mixed-state description, we also investigate and quantify the effect of experimental noise and demonstrate large-scale error mitigation.

The MPO representation of a quantum state $\sigma$ is specified by a set of $N$ tensors $M^{(j)}$ as

*Contact author: votto@mit.edu

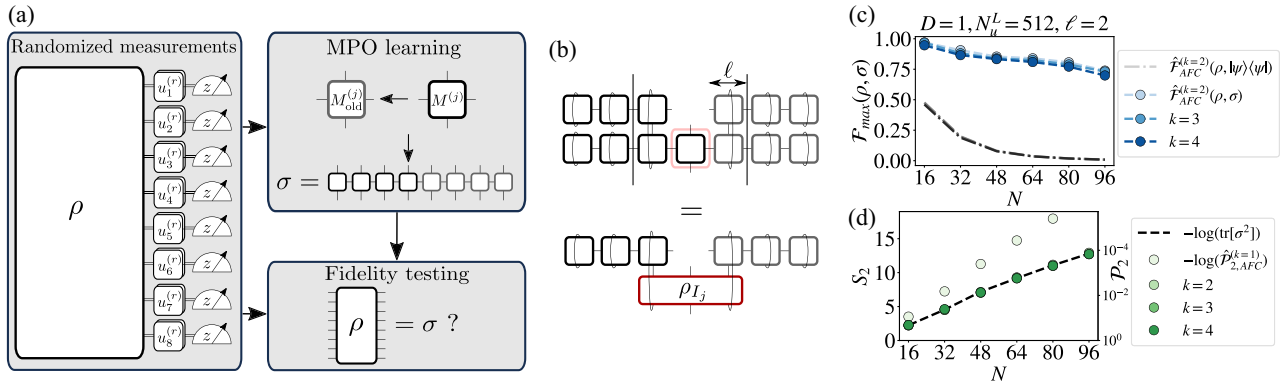


FIG. 1. Learning protocol. (a) We present a protocol to learn the MPO representation $\sigma$ of an experimental quantum state $\rho$ from two randomized measurement datasets. We use the first dataset to optimize $\sigma$, and the second one to benchmark the output $\sigma$ by estimating the fidelity $\mathcal{F}_{\max}(\rho,\sigma)$. (b) We optimize each tensor $M^{(j)}$ by solving the linear system Eq. (4), represented diagrammatically. Note that this requires experimental data depending only on the reduced density matrix $\rho_{I_j}$, where $I_j=[j-\ell,j+\ell]$. (c) We experimentally demonstrate the protocol by learning the state of the first $N$ qubits out of $N_{\text{tot}}=96$ qubits on a superconducting quantum processor, where $\rho$ is obtained by implementing Eq. (8) at depth $D=1$. We set $(\ell,\chi')=(2,4)$ in the learning algorithm, and use a total of $N_u\times N_M=2048\times 1024$ measurements. We compare the AFC fidelity [Eq. (7)] of the experimental state $\rho$ with the learned MPO $\sigma$ (marked lines) and with the target state $|\psi\rangle$ (dotted lines). (d) We estimate the Rényi entropy $S_2$ using both our protocol (dashed line) and the testing set using AFC (markers).

$$\sigma=\sum_{\{s_j\},\{s'_j\}} M^{(1)}_{s_1,s'_1}M^{(2)}_{s_2,s'_2}\ldots M^{(N)}_{s_N,s'_N}|\{s_j\}\rangle\langle\{s'_j\}|, \quad (1)$$

$$\mathcal{F}_{\max}(\rho,\sigma)=\frac{\text{tr}[\rho\sigma]}{\max(\text{tr}[\rho^2],\text{tr}[\sigma^2])}, \quad (2)$$

where $|\{s_j\}\rangle=\otimes_{j=1}^{N}|s_j\rangle$, with $s_j=0,1$, the computational basis corresponding to the Hilbert space of $N$ qubits, while $M^{(j)}_{s_j,s'_j}$ are $\chi_j\times\chi_{j+1}$ matrices. The bond dimension $\chi=\max(\chi_j)$ controls the expressivity of this ansatz [36]: while an MPO with $\chi=2^N$ can describe any quantum state, typical noisy [31–33] or thermal [34] quantum states in one dimension only require $\chi=O(1)$. Other approaches to quantum state tomography based on MPO have been proposed in recent years. They consist of either numerical methods without analytical performance guarantees [37–41], or provably efficient proposals [(i)] [42–47], but incompatible with local randomized measurements [(ii)] or the robust classical shadow framework [(iii)]. Similar considerations apply to protocols for the tomography of Gibbs states [48–55], another candidate ansatz to learn mixed states in experiments [56]. Here, we obtain properties (i)–(iii) by combining bounds on statistical errors from the classical shadow framework with the analytical properties and computational efficiency of MPOs.

Our protocol is illustrated in Fig. 1: we perform randomized measurements on the state $\rho$ in $N_u=N_u^L+N_u^T$ random bases with $N_M$ shots per basis, and assign $N_u^L$ bases to the learning set, and $N_u^T$ bases to the testing set. The learning set serves as input for a tensor network learning algorithm where each tensor of a MPO $\sigma$ is optimized sequentially, similarly to density-matrix renormalization group (DMRG) and related approaches [35,57–59]. Then, we use the testing set to benchmark the result by estimating the max fidelity, which shares key properties with the more common Uhlmann-Jozsa fidelity [60,61], and can be estimated using classical shadows [24]. Importantly, we prove that the optimization of the tensors $M^{(j)}$ and the estimation of $\mathcal{F}_{\max}(\rho,\sigma)$ can be performed with $O(\text{poly}(N))$ measurements under mild technical assumptions. In the remainder of the manuscript we illustrate our protocol and its experimental implementation, together with a demonstration and discussions of possible applications.

*Learning algorithm*—In order to illustrate and justify all the steps of our algorithm, we make some assumptions on the target state $\rho$ to be learned: (a) $\rho$ is a MPO with a bond dimension $\chi$, and (b) both the density matrices $\rho$ and $\rho'\propto\rho^2$ have finite, i.e. $O(1)$, correlation lengths. The latter assumption allows for an efficient estimation of fidelities, as we discuss later, and implies the following approximate factorization conditions (AFC) for the purity [21,55]:

$$\left|\text{tr}[\rho^2_{ABC}]^{-1}\frac{\text{tr}[\rho^2_{AB}]\text{tr}[\rho^2_{BC}]}{\text{tr}[\rho^2_B]}-1\right|\leq\alpha e^{-|B|/\xi^{(2)}_\rho}, \quad (3)$$

where $\alpha>0$ is a constant, $\xi^{(2)}_\rho=O(1)$ is the correlation length of $\rho'\propto\rho^2$, and $\rho_I=\text{tr}_{\bar{I}}[\rho]$, where $A$, $B$, and $C$ form a tripartition for a connected subset of qubits. The correlation length $\xi^{(2)}_\rho$ is also referred to as the Rényi-Markov length of $\rho$ [62,63]. Note that $\xi^{(2)}_\rho$ is not related to the injectivity length of matrix-product states (MPSs) [64], which is the relevant length scale in MPS tomography [65,66]. Later, we

will comment on the applicability of our method when these assumptions are only approximately met.

The learning algorithm starts from an initial MPO ansatz $\sigma$ with a given bond dimension $\chi'$. Then, we sequentially update the tensors $M^{(j)}$ in Eq. (1) by maximizing the geometric-mean (GM) fidelity $\mathcal{F}_{\mathrm{GM}}(\rho,\sigma)=(\mathrm{tr}[\rho\sigma]/\sqrt{\mathrm{tr}[\rho^2]\mathrm{tr}[\sigma^2]})$ [24,61]. Unlike the max fidelity, the GM fidelity is differentiable, but it is insensitive to certain types of decoherence [24,67]. The key result of this Letter is that, if $\rho$ is an MPO satisfying the assumptions above, and given a parameter $\ell > O(\xi_\rho^{(2)})$, the tensor $M^{(j)}$ that maximizes the GM fidelity approximately satisfies [67,68]

$$\mathrm{tr}_{I_j\setminus\{j\}}[\sigma_{I_j}\partial_{M^{(j)}}\sigma_{I_j}]=\mathrm{tr}_{I_j\setminus\{j\}}[\rho_{I_j}\partial_{M^{(j)}}\sigma_{I_j}], \tag{4}$$

where the trace is taken over all the qubits in $I_j$ but $j$, and $I_j=[j-\ell, j+\ell]$; see Fig. 1(b) for a diagrammatic representation. More specifically, when the algorithm is close to convergence, we can prove that $||M^{(j)}-\tilde{M}^{(j)}||_2 = O(\mathrm{tr}[\rho_{I_j}\sigma_{I_j}]\chi e^{-\ell/2\xi_{\rho\sigma}})$, where $\tilde{M}^{(j)}$ is the tensor solving Eq. (4), and $\xi_{\rho\sigma}$ is the correlation length of the operator $\rho\sigma$. This approximate update is convenient, since the right-hand side of Eq. (4) can be estimated efficiently via classical shadows, as we show later.

For each tensor, Eq. (4) can be solved numerically as a linear system in $M^{(j)}$ if $\chi' \le 4^\ell$ [67]. The algorithm then proceeds by sweeping through the tensors $M^{(j)}$ from $j=1$ to $j=N$ and back, performing a total of $N_S$ sweeps. After each sweep, we estimate $\mathcal{F}_{\max}(\rho,\sigma)$, which is the control parameter of the algorithm. Importantly, it is not necessary to know the values of $\xi_\rho^{(2)}$ and $\chi$ exactly: in order for the algorithm to accurately reconstruct $\rho$, it is only necessary that $\ell > O(\xi_\rho^{(2)})$ and $\chi' \ge \chi$ (however, similarly to MPS tomography [65,66,69,70], the number of measurements and postprocessing operations increase with them). When $\rho$ is only approximately described by a MPO with bond dimension $\chi$, we could use this approach until we reach the desired accuracy, which will be constrained by truncation errors.

*Randomized measurement protocol*—At this stage, we are left with the task of estimating (a) the right-hand side of Eq. (4) and (b) $\mathcal{F}_{\max}(\rho,\sigma)$ using respectively the learning and the testing set of randomized measurements obtained from $\rho$. A key feature of randomized measurements is that we can re-evaluate both these functions for any $\sigma$ using the same dataset. For simplicity, we will consider local randomized measurements. Using the classical shadow formalism [27], we can estimate $\mathrm{tr}_{I_j\setminus\{j\}}[\rho_{I_j}\partial_{M^{(j)}}\sigma_{I_j}]$ as $(1/N_u^L N_M)\sum_{r=1}^{N_u^L N_M}\mathrm{tr}_{I_j\setminus\{j\}}[\hat{\rho}_{I_j}^{(r)}\partial_{M^{(j)}}\sigma_{I_j}]$, where each

$$\hat{\rho}_{I_j}^{(r)}=\bigotimes_{j\in I_j}\left(3u_j^{(r)\dagger}|s_j^{(r)}\rangle\langle s_j^{(r)}|u_j^{(r)}-\mathbb{I}_j\right) \tag{5}$$

is a classical shadow of $\rho_{I_j}$. Here, $\{s_j^{(r)}=0,1\}$ are the measurement outcomes in the computational basis, $u_j^{(r)}$ are the random unitary transformations applied to each qubit $j$, and $\mathbb{I}_j$ is the identity. Crucially, this estimation can be done in norm $-2$ error $\varepsilon$ with $N_u^L = O(2^{2\ell}\chi'\varepsilon^{-2})$ measurement bases [67,71]. Note that $N_u^L$ is exponential in $\ell$, but independent of $N$. This implies that statistical errors in learning each $M^{(j)}$ can be made arbitrarily small with a number of measurements that does not grow with the total system size. One could further reduce $N_u^L$ by employing "shallow shadows," obtained by applying a shallow quantum circuits before measurements [72–78].

We now propose a scheme to estimate $\mathcal{F}_{\max}(\rho,\sigma)$ [Eq. (2)] with a controlled measurement budget. While its estimation generally requires $N_u^T N_M = O(4^N)$ randomized measurements [18,24,25], it is possible to drastically reduce this overhead under the previous assumption that the correlation lengths $\xi_\rho^{(2)}$ and $\xi_{\rho\sigma}$ are finite. In this case, we prove that [67]

$$\mathrm{tr}[\rho\sigma]\simeq\mathcal{O}_{\mathrm{AFC}}^{(k)}(\rho,\sigma)=\frac{\prod_{j=1}^{\lfloor N/k\rfloor-1}\mathrm{tr}[\rho_{A_jA_{j+1}}\sigma_{A_jA_{j+1}}]}{\prod_{j=2}^{\lfloor N/k\rfloor-1}\mathrm{tr}[\rho_{A_j}\sigma_{A_j}]}, \tag{6}$$

where $A_j$ are neighboring regions with $|A_j|=k>O(\xi_{\rho\sigma})$. The same assumptions yield a similar result for the purity, i.e., $\mathrm{tr}[\rho^2]\simeq\mathcal{P}_{2,\mathrm{AFC}}^{(k)}(\rho)=\mathcal{O}_{\mathrm{AFC}}^{(k)}(\rho,\rho)$ [21]. Defining the AFC max fidelity

$$\mathcal{F}_{\mathrm{AFC}}^{(k)}(\rho,\sigma)=\frac{\mathcal{O}_{\mathrm{AFC}}^{(k)}(\rho,\sigma)}{\max[\mathcal{P}_{2,\mathrm{AFC}}^{(k)}(\rho),\mathcal{P}_{2,\mathrm{AFC}}^{(k)}(\sigma)]}, \tag{7}$$

Eq. (6) yields $\mathcal{F}_{\max}(\rho,\sigma)\simeq\mathcal{F}_{\mathrm{AFC}}^{(k)}(\rho,\sigma)$. This approximation finally allows us to estimate $\mathcal{F}_{\max}(\rho,\sigma)$ efficiently. Indeed, $N_u^T N_M = O(4^{2k}N^3)$ measurements are sufficient to estimate $\mathcal{F}_{\mathrm{AFC}}^{(k)}(\rho,\sigma)$ with finite statistical errors, while the systematic error $|\mathcal{F}_{\max}(\rho,\sigma)-\mathcal{F}_{\mathrm{AFC}}^{(k)}(\rho,\sigma)|$ decreases exponentially with $k$ [21,67]. Now, we can quantitatively test the output $\sigma$ of the learning algorithm by estimating $\mathcal{F}_{\mathrm{AFC}}^{(k)}(\rho,\sigma)$ for various $k\ge\ell$. Note that this method relies on the assumption that $\rho$ satisfies AFC for some finite $k$, and, in contrast to MPS verification [65,66], the efficient verification of AFC is an open problem.

*Experimental results*—We now demonstrate the practical feasibility of our protocol by learning entangled quantum states from a partition of $N_{\mathrm{tot}}=96$ qubits of the IBM Brisbane superconducting quantum processor. We prepare entangled states by running the kicked Ising model quantum circuit at low depth $D$, defined as [79]

$$|\psi\rangle = \left(\prod_{j=1}^{N_{\rm tot}-1} e^{i\frac{\pi}{4}Z_jZ_{j+1}} \prod_{j=1}^{N_{\rm tot}} e^{-i\frac{\pi}{8}X_j}\right)^D |0\rangle^{\otimes N}, \qquad (8)$$

where $X_j$, $Y_j$, $Z_j$ are Pauli operators. However, the preparation and the detection of the target state $|\psi\rangle$ are affected by experimental noise, resulting in the observation of a mixed state $\rho$ which we analyze with our protocol.

For $D = 1$ and $D = 2$, we perform local randomized measurements with $N_M = 1024$ shots per basis and $N_u^L + N_u^T = 2048 \times D$ bases, and postprocess the experimental data with the previously introduced learning algorithm. As a slight modification, we perform two-site updates (instead of one-site updates) of the tensors $M^{(j)}$, as this allows us to dynamically increase the bond dimension up to $\chi'$ [67]. In addition, we implement common randomized measurements in the estimation of Eq. (4) to reduce statistical errors [80] (although this step does not drastically change the results [67]). We always initialize the algorithm in the ansatz $\sigma = (\mathbb{I}/2)^{\otimes N}$ and perform $N_S = 20$ sweeps.

We report the results in Figs. 1 and 2. First, we benchmark the results of the algorithm by comparing the fidelities $\mathcal{F}_{\max}(\rho,\sigma)$ and $\langle\psi|\rho|\psi\rangle$. We observe that $\mathcal{F}_{\max}(\rho,\sigma) \gg \langle\psi|\rho|\psi\rangle$, meaning that the learned MPO $\sigma$ correctly captures the effect of experimental noise. For $N = 96$ and $D = 1, 2$ we obtain fidelities of $\mathcal{F}_{\max}(\rho,\sigma) \sim 75\%$ and $\sim 50\%$ respectively, mainly due to statistical errors (as we similarly observe in numerical examples [67]). In a product state, the observed values would correspond to a fidelity per qubit $(\mathcal{F}_{\max}(\rho,\sigma))^{1/N} > 99\%$. Additionally, we study the magnetization $\langle Z_j\rangle$ and the two-body correlation functions $\langle Y_jY_{j+d}\rangle$, see Figs. 2(c) and 2(d). We compute them for the states $\rho, \sigma$ and $|\psi\rangle$, using standard shadow estimation [27] from the testing set for the former. We observe that the expectation values obtained from $\rho$ and $\sigma$ are in good agreement, and both highlight nonideal features of the experimental quantum state.

These observations corroborate that $\rho$ is well described by a mixed state. To quantify this feature, we now analyze the second Rényi entropy $S_2(\rho) = -\log(\mathrm{tr}[\rho^2])$ [81] of the full state, which can also be estimated using randomized measurements together with AFC [21]. In Figs. 1(d) and 2(b) we compare its AFC estimate $-\log(\mathcal{P}^{(k)}_{2,\mathrm{AFC}})$ from the testing set with $S_2(\sigma)$, observing that they are in perfect agreement at large $k$. While previous experimental approaches were limited to $N = 12$, 13 qubits [30,82], here we measure large-scale entropies to a high degree of accuracy, that correspond to exponentially small purities. By doing so we observe that the entropy of these states obeys a weak-volume law $S_2 \simeq \alpha N$, where the coefficient $\alpha \simeq 0.14$–$0.15$, compared to $\alpha = 1$ for a fully mixed state. The modest increase of the global entropy from $D = 1$ to $D = 2$ suggests that readout errors are dominant in the low-depth regime. Overall, these results demonstrate experimental tomography of $N = 96$ qubits entangled quantum states, going beyond the state-of-the-art of $N = 20$ qubits obtained for MPS [69] and Gibbs states [51].

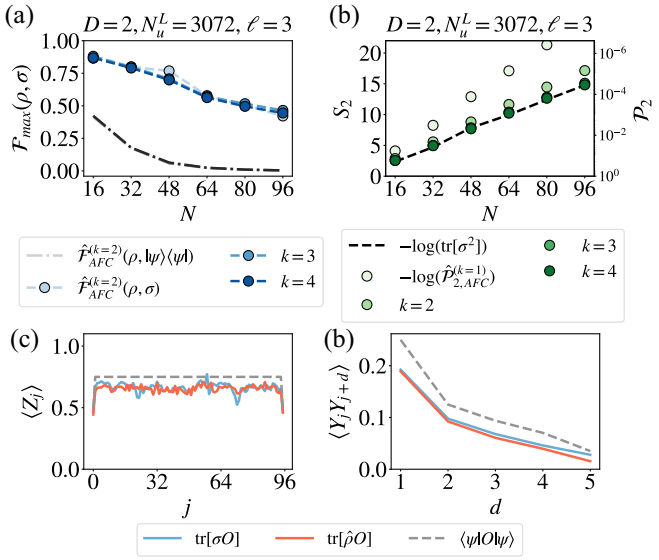


FIG. 2. Experimental results. Results for a kicked Ising model with depth $D = 2$, $N_u^L + N_u^T = 4096$ and $N_M = 1024$, and $(\ell, \chi') = (3, 8)$. (a) $\mathcal{F}_{\max}$ as a function of $N$, with respect to the experimental quantum state (markers) and the ideal target state (dotted line). (b) Global purity as a function of $N$, obtained from the learned MPO $\sigma$ (dashed line) and from the testing set using Eq. (6) (markers). (c),(d) Expectation values of the magnetization and two-body correlation functions (averaged over $j \in [3, 88]$), comparing values obtained from the learning protocol (blue lines), classical shadows from the testing set (red lines), and the pure state $|\psi\rangle$ (dashed lines).

*Application: Quantum error mitigation*—We now leverage the access to a MPO description of $\rho$ to perform quantum error mitigation. Quantum error mitigation consists in partially removing the effect of errors in the estimation of properties from a quantum experiment via classical post-processing [83]. Conventional approaches are usually based on assuming specific noise models [84], or require additional experiments [85–88]. Our approach consists instead in quantum principal component analysis (QPCA) [89,90], where we mitigate experimental noise by reconstructing the pure state $|\psi_0^\rho\rangle$ with the largest eigenvalue in the spectral decomposition $\rho = \sum_a \Lambda_a |\psi_a^\rho\rangle\langle\psi_a^\rho|$, where $\Lambda_a > \Lambda_{a+1}$ [91]. While this idea is powerful, it has been implemented only approximately by virtual distillation [92–95].

Here we perform QPCA by running the DMRG algorithm [35] on the MPO $H = -\sigma$, obtaining the state $|\psi_0^\sigma\rangle$ as a MPS. Note that this approach does not require additional experiments nor data analysis. In Fig. 3 we illustrate the results of DMRG-QPCA on the experimental data using $N = N_{\rm tot}$ [96]. In this way, we obtain $|\psi_0^\sigma\rangle$ for $D = 1$, 2, and their corresponding eigenvalues $\Lambda_0 = 9.11 \times 10^{-3}, 3.13 \times 10^{-3}$. Remarkably, we obtain high fidelities between the MPSs $|\psi_0^\sigma\rangle$ and the target states $|\psi\rangle$, even larger than 90% for

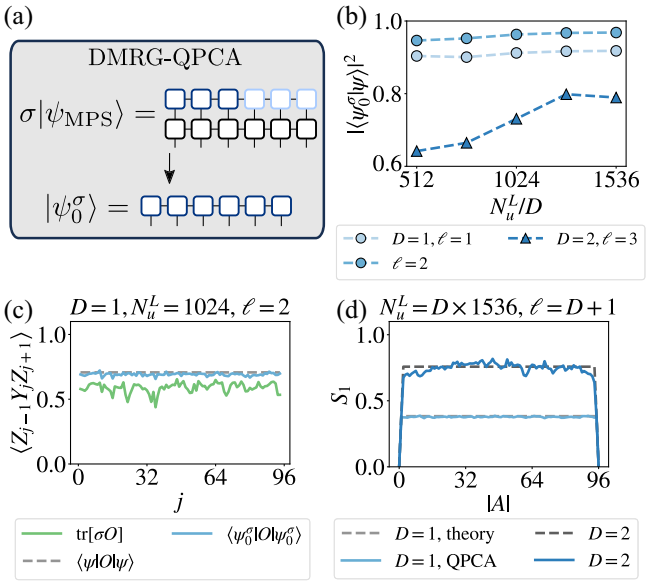


FIG. 3. Experimental quantum principal component analysis. (a) Running the DMRG algorithm on $H=-\sigma$ allows us to approximately find the principal component $|\psi_0^\sigma\rangle$, which approximates the principal component of the experimental state $\rho$. (b) Fidelity between $|\psi_0^\sigma\rangle$ and the target state $|\psi\rangle$ for the experiment at depth $D=1$, as a function of $\ell$ and $N_u$. (c) Expectation values of a local observable for depth $D=1$, compared between the learned MPO $\sigma$ and the error-mitigated state to the theory prediction. (d) Bipartite Von Neumann entropy as a function of the cut for $D=1, 2$, compared between $|\psi_0^\sigma\rangle$ and $|\psi\rangle$.

$D=1$, corroborating the power of this error mitigation method. This is also reflected by expectation values of local observables, that show a dramatic improvement from the MPO prediction of $\sigma$. Finally, we leverage the MPS representation to observe the growth of the bipartite von Neumann entropy $S_1=\mathrm{tr}_A[\rho'\log\rho']$ with the circuit depth, where we take $\rho'=\mathrm{tr}_{\bar{A}}[|\psi_0^\sigma\rangle\langle\psi_0^\sigma|]$ and $A=[1,|A|]$; see Fig. 3(d). These results experimentally demonstrate QPCA at large scales, and provide a strong case for the application of our learning protocol to quantum error mitigation.

*Conclusions and outlook*—Our protocol provides a quantum-to-classical converter [97] that compresses $N_uN_M$ randomized measurement outcomes from an experimental quantum state $\rho$ in a single classical object, the MPO $\sigma$. Having access to an MPO approximation of $\rho$ not only allows us to estimate several physical properties efficiently [35], i.e., without reprocessing experimental data each time [13], but also to apply powerful error-mitigation based on tensor-network algorithms.

Our ability to combine quantum experiments with classical tensor-network methods opens up further possibilities. For instance, MPO tomography can be associated with MPS preparation algorithms which take as input an MPO $\sigma$ represented classically and devise the quantum circuit that efficiently forms the corresponding state $\rho$ in a universal quantum computer [98,99]. This gives us the possibility to interact with a quantum system multiple times, or even connect different experiments to perform quantum computing beyond the possibilities of each individual device.

An interesting use case consists in quantum circuit cutting: by saving an intermediate state of a quantum algorithm as a MPO and performing QPCA on it, one could resume the quantum algorithm by reloading the (error-mitigated) state with a MPS preparation circuit. Another concrete application consists in modular experiments where a fault-tolerant quantum computer is used to analyze the state of a noisy quantum simulator. For instance, one could prepare a quantum state of interest in a quantum simulation experiment, and perform MPO tomography, then use a quantum circuit to prepare its MPS purification on a fault-tolerant quantum computer, and finally apply a quantum algorithm to measure the von Neumann entropy [100–102].

*Acknowledgments*—We acknowledge insightful discussions with Antoine Browaeys, Mari Carmen Bañuls, Soonwon Choi, Thierry Lahaye, Daniel Stilck-França, Georgios Styliaris, and Xavier Waintal. The experimental data have been collected using the Qiskit library [103], and have been postprocessed using the RandomMeas [104] and ITensor [105] libraries. The work of M. V. and B. V. was funded by the French National Research Agency via the JCJC project QRand (No. ANR-20-CE47-0005), and via the research programs Plan France 2030 EPIQ (No. ANR-22-PETQ-0007), QUBITAF (No. ANR-22-PETQ-0004), and HQI (No. ANR-22-PNCQ-0002). We acknowledge the use of IBM Quantum Credits for this work. M. L. acknowledges support by the Deutsche Forschungsgemeinschaft (DFG, German Research Foundation) under Germany's Excellence Strategy—EXC-2111–390814868. The work of C. L. was funded by the French National Research Agency via the PRC project ESQuisses (No. ANR-20-CE47-0014-01). J. I. C. acknowledges funding from the Federal Ministry of Education and Research Germany (BMBF) via the project FermiQP (No. 13N15889). Work at MPQ is part of the Munich Quantum Valley, which is supported by the Bavarian state government with funds from the Hightech Agenda Bayern Plus. P. Z. acknowledges support by the European Union's Horizon Europe research and innovation program under Grant Agreement No. 101113690 (PASQANS2). The work of L. P. was funded by the European Union (ERC, QUANTHEM, No. 101114881). We acknowledge support by the Erwin Schrödinger International Institute for Mathematics and Physics (ESI).

The views expressed are those of the authors, and do not reflect the official policy or position of IBM or the IBM Quantum team. Views and opinions expressed are however those of the author(s) only and do not necessarily reflect those of the European Union or the European Research Council Executive Agency. Neither the European Union nor the granting authority can be held responsible for them.

*Data availability*—The experimental data processed in this work have been deposited in a dedicated Zenodo repository [106].


[1] R. Blatt and C. F. Roos, Nat. Phys. **8**, 277 (2012).
[2] C. Gross and I. Bloch, Science **357**, 995 (2017).
[3] J. Preskill, Quantum **2**, 79 (2018).
[4] F. Schäfer, T. Fukuhara, S. Sugawa, Y. Takasu, and Y. Takahashi, Nat. Rev. Phys. **2**, 411 (2020).
[5] M. Kjaergaard, M. E. Schwartz, J. Braumüller, P. Krantz, J. I.-J. Wang, S. Gustavsson, and W. D. Oliver, Annu. Rev. Condens. Matter Phys. **11**, 369 (2020).
[6] E. Altman *et al.*, PRX Quantum **2**, 017003 (2021).
[7] M. Morgado and S. Whitlock, AVS Quantum Sci. **3**, 023501 (2021).
[8] C. Monroe, W. C. Campbell, L.-M. Duan, Z.-X. Gong, A. V. Gorshkov, P. W. Hess, R. Islam, K. Kim, N. M. Linke, G. Pagano, P. Richerme, C. Senko, and N. Y. Yao, Rev. Mod. Phys. **93**, 025001 (2021).
[9] Y. Alexeev *et al.*, PRX Quantum **2**, 017001 (2021).
[10] E. Pelucchi, G. Fagas, I. Aharonovich, D. Englund, E. Figueroa, Q. Gong, H. Hannes, J. Liu, C.-Y. Lu, N. Matsuda, J.-W. Pan, F. Schreck, F. Sciarrino, C. Silberhorn, J. Wang, and K. D. Jöns, Nat. Rev. Phys. **4**, 194 (2022).
[11] G. Burkard, T. D. Ladd, A. Pan, J. M. Nichol, and J. R. Petta, Rev. Mod. Phys. **95**, 025003 (2023).
[12] A. Elben, B. Vermersch, C. F. Roos, and P. Zoller, Phys. Rev. A **99**, 052323 (2019).
[13] A. Elben, S. T. Flammia, H.-Y. Huang, R. Kueng, J. Preskill, B. Vermersch, and P. Zoller, Nat. Rev. Phys. **5**, 9 (2022).
[14] P. Cieśliński, S. Imai, J. Dziewior, O. Gühne, L. Knips, W. Laskowski, J. Meinecke, T. Paterek, and T. Vértesi, Phys. Rep. **1095**, 1 (2024).
[15] T. Brydges, A. Elben, P. Jurcevic, B. Vermersch, C. Maier, B. P. Lanyon, P. Zoller, R. Blatt, and C. F. Roos, Science **364**, 260 (2019).
[16] A. Elben, R. Kueng, H.-Y. R. Huang, R. van Bijnen, C. Kokail, M. Dalmonte, P. Calabrese, B. Kraus, J. Preskill, P. Zoller, and B. Vermersch, Phys. Rev. Lett. **125**, 200501 (2020).
[17] A. Neven, J. Carrasco, V. Vitale, C. Kokail, A. Elben, M. Dalmonte, P. Calabrese, P. Zoller, B. Vermersch, R. Kueng, and B. Kraus, npj Quantum Inf. **7**, 152 (2021).
[18] A. Rath, C. Branciard, A. Minguzzi, and B. Vermersch, Phys. Rev. Lett. **127**, 260501 (2021).
[19] A. Rath, V. Vitale, S. Murciano, M. Votto, J. Dubail, R. Kueng, C. Branciard, P. Calabrese, and B. Vermersch, PRX Quantum **4**, 010318 (2023).
[20] J. Carrasco, M. Votto, V. Vitale, C. Kokail, A. Neven, P. Zoller, B. Vermersch, and B. Kraus, Phys. Rev. A **109**, 012422 (2024).
[21] B. Vermersch, M. Ljubotina, J. I. Cirac, P. Zoller, M. Serbyn, and L. Piroli, Phys. Rev. X **14**, 031035 (2024).
[22] M. P. da Silva, O. Landon-Cardinal, and D. Poulin, Phys. Rev. Lett. **107**, 210404 (2011).
[23] S. T. Flammia and Y.-K. Liu, Phys. Rev. Lett. **106**, 230501 (2011).
[24] A. Elben, B. Vermersch, R. van Bijnen, C. Kokail, T. Brydges, C. Maier, M. K. Joshi, R. Blatt, C. F. Roos, and P. Zoller, Phys. Rev. Lett. **124**, 010504 (2020).
[25] D. Zhu, Z. P. Cian, C. Noel, A. Risinger, D. Biswas, L. Egan, Y. Zhu, A. M. Green, C. H. Alderete, N. H. Nguyen, Q. Wang, A. Maksymov, Y. Nam, M. Cetina, N. M. Linke, M. Hafezi, and C. Monroe, Nat. Commun. **13**, 2315 (2022).
[26] H.-Y. Huang, J. Preskill, and M. Soleimanifar, Nat. Phys. **21**, 1834 (2025).
[27] H.-Y. Huang, R. Kueng, and J. Preskill, Nat. Phys. **16**, 1050 (2020).
[28] D. E. Koh and S. Grewal, Quantum **6**, 776 (2022).
[29] S. Chen, W. Yu, P. Zeng, and S. T. Flammia, PRX Quantum **2**, 030348 (2021).
[30] V. Vitale, A. Rath, P. Jurcevic, A. Elben, C. Branciard, and B. Vermersch, PRX Quantum **5**, 030338 (2024).
[31] K. Noh, L. Jiang, and B. Fefferman, Quantum **4**, 318 (2020).
[32] S. Cheng, C. Cao, C. Zhang, Y. Liu, S.-Y. Hou, P. Xu, and B. Zeng, Phys. Rev. Res. **3**, 023005 (2021).
[33] F. Verstraete, J. J. García-Ripoll, and J. I. Cirac, Phys. Rev. Lett. **93**, 207204 (2004).
[34] T. Kuwahara, A. M. Alhambra, and A. Anshu, Phys. Rev. X **11**, 011047 (2021).
[35] U. Schollwöck, Ann. Phys. (Amsterdam) **326**, 96 (2011).
[36] J. Guth Jarkovský, A. Molnár, N. Schuch, and J. I. Cirac, PRX Quantum **1**, 010304 (2020).
[37] T. Baumgratz, A. Nüßeler, M. Cramer, and M. B. Plenio, New J. Phys. **15**, 125004 (2013).
[38] A. Lidiak, C. Jameson, Z. Qin, G. Tang, M. B. Wakin, Z. Zhu, and Z. Gong, arXiv:2207.06397.
[39] G. Torlai, C. J. Wood, A. Acharya, G. Carleo, J. Carrasquilla, and L. Aolita, Nat. Commun. **14**, 2858 (2023).
[40] Y. Guo and S. Yang, Commun. Phys. **7**, 322 (2024).
[41] C. Jameson, Z. Qin, A. Goldar, M. B. Wakin, Z. Zhu, and Z. Gong, arXiv:2408.07115.
[42] T. Baumgratz, D. Gross, M. Cramer, and M. B. Plenio, Phys. Rev. Lett. **111**, 020401 (2013).
[43] M. Holzäpfel, M. Cramer, N. Datta, and M. B. Plenio, J. Math. Phys. (N.Y.) **59**, 042201 (2018).
[44] Z. Qin, C. Jameson, Z. Gong, M. B. Wakin, and Z. Zhu, IEEE Trans. Inf. Theory **70**, 5030 (2024).
[45] Z. Qin, C. Jameson, A. Goldar, M. B. Wakin, Z. Gong, and Z. Zhu, arXiv:2410.02583.
[46] M. Fanizza, N. Galke, J. Lumbreras, C. Rouzé, and A. Winter, arXiv:2312.07516.
[47] Z. Qin, J. M. Lukens, B. T. Kirby, and Z. Zhu, npj Quantum Inf. **11**, 147 (2025).
[48] B. Swingle and I. H. Kim, Phys. Rev. Lett. **113**, 260501 (2014).
[49] A. Anshu, S. Arunachalam, T. Kuwahara, and M. Soleimanifar, Nat. Phys. **17**, 931 (2021).
[50] C. Kokail, R. van Bijnen, A. Elben, B. Vermersch, and P. Zoller, Nat. Phys. **17**, 936 (2021).
[51] M. K. Joshi, C. Kokail, R. van Bijnen, F. Kranzl, T. V. Zache, R. Blatt, C. F. Roos, and P. Zoller, Nature (London) **624**, 539 (2023).
[52] C. Rouzé and D. Stilck França, Quantum **8**, 1319 (2024).

[53] J. Haah, R. Kothari, and E. Tang, Nat. Phys. **20**, 1027 (2024).

[54] A. Bakshi, A. Liu, A. Moitra, and E. Tang, *Proceedings of the 56th Annual ACM Symposium on Theory of Computing STOC 2024* (2024), pp. 1470–1477.

[55] Ángela Capel, Álvaro M. Alhambra, P. Gondolf, A. R. de Alarcón, and S. O. Scalet, arXiv:2402.18500.

[56] A. Anshu and S. Arunachalam, Nat. Rev. Phys. **6**, 59 (2024).

[57] E. Stoudenmire and D. J. Schwab, Adv. Neural Inf. Process. Syst. **29**, 4799 (2016).

[58] Z.-Y. Han, J. Wang, H. Fan, L. Wang, and P. Zhang, Phys. Rev. X **8**, 031012 (2018).

[59] T. Ayral, T. Louvet, Y. Zhou, C. Lambert, E. M. Stoudenmire, and X. Waintal, PRX Quantum **4**, 020304 (2023).

[60] R. Jozsa, J. Mod. Opt. **41**, 2315 (1994).

[61] Y.-C. Liang, Y.-H. Yeh, P. E. M. F. Mendonça, R. Y. Teh, M. D. Reid, and P. D. Drummond, Rep. Prog. Phys. **82**, 076001 (2019).

[62] S. Sang and T. H. Hsieh, Phys. Rev. Lett. **134**, 070403 (2025).

[63] C. Zhang, Y. Xu, J.-H. Zhang, C. Xu, Z. Bi, and Z.-X. Luo, Phys. Rev. B **111**, 115137 (2025).

[64] J. I. Cirac, D. Pérez-García, N. Schuch, and F. Verstraete, Rev. Mod. Phys. **93**, 045003 (2021).

[65] M. Cramer, M. B. Plenio, S. T. Flammia, R. Somma, D. Gross, S. D. Bartlett, O. Landon-Cardinal, D. Poulin, and Y.-K. Liu, Nat. Commun. **1**, 149 (2010).

[66] B. P. Lanyon, C. Maier, M. Holzäpfel, T. Baumgratz, C. Hempel, P. Jurcevic, I. Dhand, A. S. Buyskikh, A. J. Daley, M. Cramer, M. B. Plenio, R. Blatt, and C. F. Roos, Nat. Phys. **13**, 1158 (2017).

[67] See Supplemental Material at http://link.aps.org/supplemental/10.1103/rbg2-f61m for further details.

[68] K. Koor, Y. Qiu, L. C. Kwek, and P. Rebentrost, arXiv:2312.04858.

[69] M. K. Kurmapu, V. V. Tiunova, E. S. Tiunov, M. Ringbauer, C. Maier, R. Blatt, T. Monz, A. K. Fedorov, and A. I. Lvovsky, PRX Quantum **4**, 040345 (2023).

[70] Y. Teng, R. Samajdar, K. Van Kirk, F. Wilde, S. Sachdev, J. Eisert, R. Sweke, and K. Najafi, PRX Quantum **6**, 040303 (2025).

[71] F. Altomare and M. Campiti, *Korovkin-Type Approximation Theory and Its Applications* (De Gruyter, Berlin, New York, 1994).

[72] M. Ippoliti, Y. Li, T. Rakovszky, and V. Khemani, Phys. Rev. Lett. **130**, 230403 (2023).

[73] C. Bertoni, J. Haferkamp, M. Hinsche, M. Ioannou, J. Eisert, and H. Pashayan, Phys. Rev. Lett. **133**, 020602 (2024).

[74] R. M. S. Farias, R. D. Peddinti, I. Roth, and L. Aolita, Quantum Sci. Technol. **10**, 025044 (2025).

[75] H.-Y. Hu, A. Gu, S. Majumder, H. Ren, Y. Zhang, D. S. Wang, Y.-Z. You, Z. Minev, S. F. Yelin, and A. Seif, Nat. Commun. **16**, 2943 (2025).

[76] R. Cioli, E. Ercolessi, M. Ippoliti, X. Turkeshi, and L. Piroli, Quantum **9**, 1698 (2025).

[77] T. Schuster, J. Haferkamp, and H.-Y. Huang, Science **389**, 92 (2025).

[78] L. Cui, T. Schuster, F. Brandao, and H.-Y. Huang, arXiv:2507.06216.

[79] Y. Kim, A. Eddins, S. Anand, K. X. Wei, E. van den Berg, S. Rosenblatt, H. Nayfeh, Y. Wu, M. Zaletel, K. Temme, and A. Kandala, Nature (London) **618**, 500 (2023).

[80] B. Vermersch, A. Rath, B. Sundar, C. Branciard, J. Preskill, and A. Elben, PRX Quantum **5**, 010352 (2024).

[81] We consider the logarithm to be in base 2, such that $S_2((\mathbb{I}/2)^{\otimes N}) = N$.

[82] T. I. Andersen, N. Astrakhantsev, A. H. Karamlou, J. Berndtsson, J. Motruk, A. Szasz, J. A. Gross, A. Schuckert, T. Westerhout, Y. Zhang *et al.*, Nature (London) **638**, 79 (2025).

[83] Z. Cai, R. Babbush, S. C. Benjamin, S. Endo, W. J. Huggins, Y. Li, J. R. McClean, and T. E. O'Brien, Rev. Mod. Phys. **95**, 045005 (2023).

[84] E. van den Berg, Z. K. Minev, A. Kandala, and K. Temme, Nat. Phys. **19**, 1116 (2023).

[85] T. Giurgica-Tiron, Y. Hindy, R. LaRose, A. Mari, and W. J. Zeng, *2020 IEEE International Conference on Quantum Computing and Engineering (QCE)* (2020), p. 306.

[86] Y. Guo and S. Yang, PRX Quantum **3**, 040313 (2022).

[87] S. Filippov, M. Leahy, M. A. C. Rossi, and G. García-Pérez, arXiv:2307.11740.

[88] S. Mangini, M. Cattaneo, D. Cavalcanti, S. Filippov, Matteo A. C. Rossi, and G. García-Pérez, Phys. Rev. Res. **6**, 033217 (2024).

[89] S. Lloyd, M. Mohseni, and P. Rebentrost, Nat. Phys. **10**, 631 (2014).

[90] H.-Y. Huang, M. Broughton, J. Cotler, S. Chen, J. Li, M. Mohseni, H. Neven, R. Babbush, R. Kueng, J. Preskill, and J. R. McClean, Science **376**, 1182 (2022).

[91] B. Koczor, New J. Phys. **23**, 123047 (2021).

[92] J. Cotler, S. Choi, A. Lukin, H. Gharibyan, T. Grover, M. E. Tai, M. Rispoli, R. Schittko, P. M. Preiss, A. M. Kaufman, M. Greiner, H. Pichler, and P. Hayden, Phys. Rev. X **9**, 031013 (2019).

[93] W. J. Huggins, S. McArdle, T. E. O'Brien, J. Lee, N. C. Rubin, S. Boixo, K. B. Whaley, R. Babbush, and J. R. McClean, Phys. Rev. X **11**, 041036 (2021).

[94] A. Seif, Z.-P. Cian, S. Zhou, S. Chen, and L. Jiang, PRX Quantum **4**, 010303 (2023).

[95] H. Hakoshima, S. Endo, K. Yamamoto, Y. Matsuzaki, and N. Yoshioka, Phys. Rev. Lett. **133**, 080601 (2024).

[96] We initialize DMRG with $|\psi_0\rangle \propto |\psi_{\mathrm{RMPS}}\rangle + \epsilon|0\rangle^{\otimes N}$ where $|\psi_{\mathrm{RMPS}}\rangle$ is a random MPS with small bond dimension, and $\epsilon \gtrsim 10^{-2}$. For $\epsilon = 0$, we numerically observe that the DMRG algorithm does not update the random MPS.

[97] H.-Y. Huang, R. Kueng, G. Torlai, V. V. Albert, and J. Preskill, Science **377**, eabk3333 (2022).

[98] D. Malz, G. Styliaris, Z.-Y. Wei, and J. I. Cirac, Phys. Rev. Lett. **132**, 040404 (2024).

[99] S. Fomichev, K. Hejazi, M. S. Zini, M. Kiser, J. Fraxanet, P. A. M. Casares, A. Delgado, J. Huh, A.-C. Voigt, J. E. Mueller, and J. M. Arrazola, PRX Quantum **5**, 040339 (2024).

[100] T. Gur, M.-H. Hsieh, and S. Subramanian, arXiv:2111.11139.

[101] A. Luongo and C. Shao, arXiv:2011.06475.

[102] V. Giovannetti, S. Lloyd, and L. Maccone, arXiv:2504.11049.
[103] A. Javadi-Abhari, M. Treinish, K. Krsulich, C. J. Wood, J. Lishman, J. Gacon, S. Martiel, P. D. Nation, L. S. Bishop, A. W. Cross, B. R. Johnson, and J. M. Gambetta, arXiv:2405.08810.
[104] A. Elben and B. Vermersch, arXiv:2509.12749.
[105] M. Fishman, S. R. White, and E. M. Stoudenmire, SciPost Phys. Codebases **2022**, 4 (2022).
[106] M. Votto, M. Ljubotina, L. Piroli, and B. Vermersch, Data for "Learning mixed quantum states in large-scale experiment", https://doi.org/10.5281/zenodo.18323569 (2026).